Dynamic in vivo Imaging of Microvasculature and Perfusion by Miniaturized Confocal Laser Microscopy

M. Goetz[a]   S. Thomas[c]   A. Heimann[b]   P. Delaney[c]   C. Schneider[a]   M. Relle[a]
A. Schwarting[a]   P.R. Galle[a]   O. Kempski[b]   M.F. Neurath[a]   R. Kiesslich[a]

[a]First Medical Clinic and [b]Institute of Neurosurgical Pathophysiology, University of Mainz, Mainz, Germany;
[c]Optiscan Pty Ltd., Notting Hill, Vic., Australia

Abstract
Introduction: Microvasculature and associated pathologies mandate dynamic imaging. We evaluated a novel miniaturized confocal laser scanning probe for in vivo visualization of blood vessels, blood flow, cell tracking and perfusion in both healthy rodents and disease models. *Methods:* The hand-held confocal microscopy system allowed a 500- to 2,400-fold magnification at a dynamically variable imaging depth. Different intravital stains were used alone or in combination for tissue, nuclear, plasma and vascular endothelial cell staining and for blood flow visualization, and targeted staining for individual cell populations. *Results:* Precision optical sectioning yielded high-resolution images in vivo. Leucocyte-endothelium interactions in brain microvasculature were followed in serial sections. A microthrombosis was identified after sequential injection of FITC-labelled erythrocytes, FITC-dextran and acriflavine. Glomerular alterations were visualized in the MRL/lpr mouse model of lupus nephritis. *Discussion:* Intravital confocal microscopy with a miniaturized hand-held probe combines high-resolution subsurface face imaging in real time for dynamic visualization of vessels, cells, blood flow and associated pathologies, permitting a truly comprehensive vascular imaging in vivo at the cellular level.
Copyright © 2008 S. Karger AG, Basel

Introduction

Blood flow, vascular morphology, cell-cell interactions and associated pathologies are processes that mandate dynamic imaging. Histopathology represents the gold standard of microscopic diagnosis in many disease entities. However, it may not be adequate to monitor such dynamic processes secondary to fixation and staining artefacts, and it usually lacks a temporal domain. Light microscopy techniques have been introduced for real-time imaging in vivo [1] but do not permit subsurface optical sectioning in whole tissue, and magnification and resolution in vivo are limited.

Confocal microscopy, introduced approximately 20 years ago, enhances spatial resolution compared with con-

Dr. Martin Goetz
First Medical Clinic
Johannes-Gutenberg-Universität
DE–55131 Mainz (Germany)
Tel. +49 6131 171, Fax +49 6131 17 6416, E-Mail mgoetz@mail.uni-mainz.de

ventional fluorescence microscopy, especially in the axial direction [2, 3]. In conjunction with fluorescent dyes, it permits observation of fine subcellular detail, even in cells located many micrometres below the tissue surface, by eliminating out-of-focus light [4]. However, the in vivo use of confocal imaging has been limited technically by the requirement to position the animal on a microscope stage precisely relative to a fixed microscope objective. This imposes physical size limitations on the animals that can be practically imaged in vivo, and relative movement between the tissue of interest and the fixed optics imposes limits on magnification and image stability. Recently, the miniaturization of a confocal scanner and its integration into a hand-held device has permitted straightforward fluorescence confocal microscopy in rodents in vivo [5–7]. The aim of the present study was to evaluate this newly developed miniaturized point scanning microscope probe for intravital dynamic visualization of tissue microvasculature, blood flow and single cells in healthy rodents and models of human vascular diseases and to establish staining protocols for high-resolution morphological and functional imaging and multi-labelling in vivo.

Methods

In vivo Confocal Imaging

The FIVE 1 fluorescence in vivo endomicroscopy system (Optiscan, Melbourne, Vic., Australia), uses a 488-nm single-line laser for fluorophore excitation in vivo. Fluorescence emission was detected at >505 nm. A hand-held probe (model RBK6315A: 5.0 mm distal tip diameter, 6.3 mm shaft diameter) was used to produce images with a field of view of $475 \times 475 \mu$m, each with a lateral resolution of <0.7 μm, and an axial resolution (optical slice thickness) of 7.0 μm. The imaging depth was dynamically variable using a foot pedal; imaging depth could be adjusted in 4-μm increments over a range of 0–250 μm below the surface of the tissue. Images were captured at a frame rate of 1.6/s at a resolution of $1,024 \times 512$ pixels or 0.8/s at $1,024 \times 1,024$ pixels. Laser power at the tissue surface was user controlled over a possible range from 0 to 1,000 μW to achieve appropriate image contrast. No major readjustments of the instrumentation were performed during the ongoing examination. Per examination, 50–500 images were captured using a foot pedal and digitally stored as 12-bit grey-scale images. Three-dimensional reconstruction from z-stacks was performed with Image J 1.30v (W. Rasband, NIH, Bethesda, Md., USA), as previously described [5].

Confocal Imaging and Animal Models

Healthy male or female mice had a C57BL/6 or FVB background. Two MRL/lpr mice (4 and 7 months old) were used as a model of lupus nephritis [8] and compared to age-matched controls. For imaging of the glomerular structure, the medulla was surgically exposed. Two Mongolian gerbils were prepared for triple staining. Animals were kept at the Animal Facility of the Uni-

versity of Mainz in a temperature-controlled environment on a 12-hour light-dark cycle and were fed regular pelleted rodent maintenance diet and water ad libitum. Animal procedures conformed to institutional standards.

For confocal imaging, animals were deeply anaesthetized using 12 ml/kg body weight avertin i.p. (1 g of 2,2,2-tribromo-ethanol per 1 ml tertiary amyl alcohol, both Sigma-Aldrich, Germany; 2.5% in phosphate-buffered saline). The organ of interest was surgically exposed. For brain imaging, the head was secured in a stereotactic frame, and a cranial fenestration was made leaving the dura intact. Images were generated by placing the confocal imaging window at the tip of the probe in direct, gentle contact with the organ of interest either by using it by hand (comparable to holding a pen) or by mounting it onto a stereotactic frame [for continuous imaging of the same field of view (fig. 3A–C) or three-dimensional reconstruction (fig. 1)]. Pathological changes within the organs were identified in vivo in real time by observing the microscopic structure of the tissue. All findings were recorded by capturing a sequence of adjacent imaging planes at sequential depths to obtain volumetric tissue sampling. After in vivo imaging, the animals were sacrificed by an avertin overdose and tissue specimens collected, where appropriate.

Staining Protocols

Confocal images were collected following systemic application of fluorescent agents. These were administered systemically to the mice via the tail vein or intracardially, and to the gerbils via an intravenous line that was placed into the left femoral vein.

Single Fluorophore Experiments

Fluorescein sodium (Alcon Pharma, Freiburg, Germany) was administered at 100 μg/g body weight. FITC-labelled dextran (MW 150 kDa, Sigma-Aldrich, Steinheim, Germany) was injected at 250 μg/g body weight. Acriflavine hydrochloride (Sigma Pharmaceuticals, Melbourne, Vic., Australia) was applied at 10 μg/g body weight. FITC-labelled *Lycopersicon esculentum* lectin (Vector, Burlingame, Calif., USA) was injected intravenously at 15 μg/g body weight.

Blood Cell Labelling

Fluorescent labelling of erythrocytes was performed as previously described [9]. In short, a gerbil was sacrificed, full blood harvested and centrifuged for 10 min. Buffy coat and plasma were removed, and red blood cells (RBCs) were washed in glucose-saline buffer. RBCs were incubated with 9 mg FITC/ml blood for 2 h and washed in buffer 5 times. Labelled RBCs were diluted to a haematocrit of 45% with normal saline and citrate-phosphate-dextrose for conservation. Then, 15 μl of the suspension were injected per 10 g body weight.

For labelling of murine lymphocytes, spleen mononuclear cells were harvested and separated by MACS® columns (Miltenyi Biotech, Bergisch-Gladbach, Germany), as described previously [10]; 10^7 cells were incubated with 10 μg FITC-labelled anti-CD3 monoclonal antibody (clone 17A2, BD Biosciences Pharmingen, San Diego, Calif., USA) for 1 h at 4°C protected from light without further fixation, and then immediately injected into a syngeneic littermate (n = 2 mice).

Murine peripheral blood mononuclear cells (PBMCs) were isolated from the spleen, incubated with acriflavine and injected into syngeneic littermates (n = 2 mice).

Dual and Triple Labelling Experiments

For dual and triple labelling, the concentrations of fluorophores were optimized to provide sufficient background contrast to allow detection while still permitting discrimination of other targeted structures at the same time. A stronger contrast was chosen for targeted imaging. Acriflavine and fluorescein were injected intravenously at 5 and 50 μg/g, respectively, to provide low-contrast background staining.

For triple label imaging of the microvasculature in the gerbil brain, an intravenous line was placed into the left femoral vein. Labelled RBCs, FITC-dextran (MW 60 kDa, Sigma, titrated up to 10 μg/g) and acriflavine (10 μg/g) were infused sequentially while simultaneously imaging the brain tissue to monitor for adequate tissue contrast from each contrast agent.

Results

Imaging of Vessel Morphology

Fluorescein sodium is a small water-soluble compound that distributes in the total body water when administered systemically. As it readily diffuses out of the microvasculature into the surrounding tissues, it yielded a good overall impression of both the microvasculature and the tissue micro-architecture after systemic application. A strong, high-contrast fluorescent signal was available within a few seconds to minutes after injection.

FITC-labelled dextran was retained in the vessel lumina due to its high molecular weight and was used for plasma staining, without labelling of the surrounding tissues. In the mouse brain, the capillary network was selectively contrasted by injection of FITC-dextran and recorded in serial sections. No brain parenchyma was contrasted due to the high-molecular-weight dextran and the intact blood-brain barrier. Image stacks over the imaging depth range were used for three-dimensional reconstruction of the capillary network. A snapshot caught at an oblique angle is rendered in figure 1A. The video version of the full spin can be found online as online supplement figure 1 (www.karger.com/doi/10.1159/000148242) and a virtual flight along the z-axis through the capillary network of the brain as online supplement figure 2 (www.karger.com/doi/10.1159/000148242).

In the gerbil brain where the intact blood-brain barrier inhibited extravasation, acriflavine labelled the nuclei and to a lesser extent the cytoplasm of the vascular endothelial cells lining the vasculature and also the nuclei of the circular smooth-muscle cells of arterioles (fig. 1B–E). In the periphery, intravenous acriflavine diffused out of the vasculature and into the surrounding tissues.

FITC-labelled *L. esculentum* lectin binds to glycoprotein moieties and therefore selectively labelled vascular endothelial cells after intravenous injection.

Triple Labelling for Vascular Morphology, Cell Tracking and Blood Flow

The simultaneous use of three fluorescent agents allowed detailed examination of the gerbil brain microvasculature in vivo (fig. 1B–E). Acriflavine was used to label the nuclei of the vasculature (vascular endothelial cells and circular smooth-muscle cells of arterioles), FITC-dextran for plasma staining to show vessel perfusion and contrast the unlabelled RBCs, and labelled RBCs were tracked to observe blood flow. Dynamic image depth adjustment was used to obtain precise optical sections through microvessels to enable a clear discrimination of arterioles from venules and capillaries. The arterioles were characterized by transverse bands of smooth muscle cell nuclei resulting in tiny retractions of the vessel walls, representing the morphological correlate of the brain vessel autoregulation site. Endothelial cell nuclei lining the lumen ran parallel to the vessel axis. A complete sequence of adjacent optical planes is rendered in online supplement figure 3 (www.karger.com/doi/10.1159/000148242). Labelled RBCs in the lumen of the larger vessels caused image artefacts, resulting in elongation or shortening depending on whether their flow was in the same or opposite direction to the Y scan (fig. 1E, inset).

Imaging of Blood Flow and Thrombosis

Blood flow was observed in real time by observation of unstained cells in FITC-dextran-stained plasma (fig. 2A). Alternatively, individual labelled RBCs were visualized in vessels after re-injection (fig. 2B). When the blood plasma was counterstained with low concentrations of FITC-dextran, both labelled and unlabelled RBCs became visible as a positive or negative contrast, respectively (fig. 2C). However, quantification of blood flow velocity was not possible because individual cells frequently moved out of the imaging plane and image acquisition speed was insufficient to follow single cells in larger vessels where the flow rate is highest.

A spontaneous microthrombosis was identified in a gerbil brain venule by confocal microscopy after sequential injection of FITC-labelled erythrocytes, FITC-dextran and acriflavine hydrochloride (fig. 2D). Blood stasis was substantiated by observing an unstained black luminal mass of non-nucleated, unstained blood cells without any visible flow of FITC-dextran-labelled plasma. FITC-labelled erythrocytes were persistently trapped within the
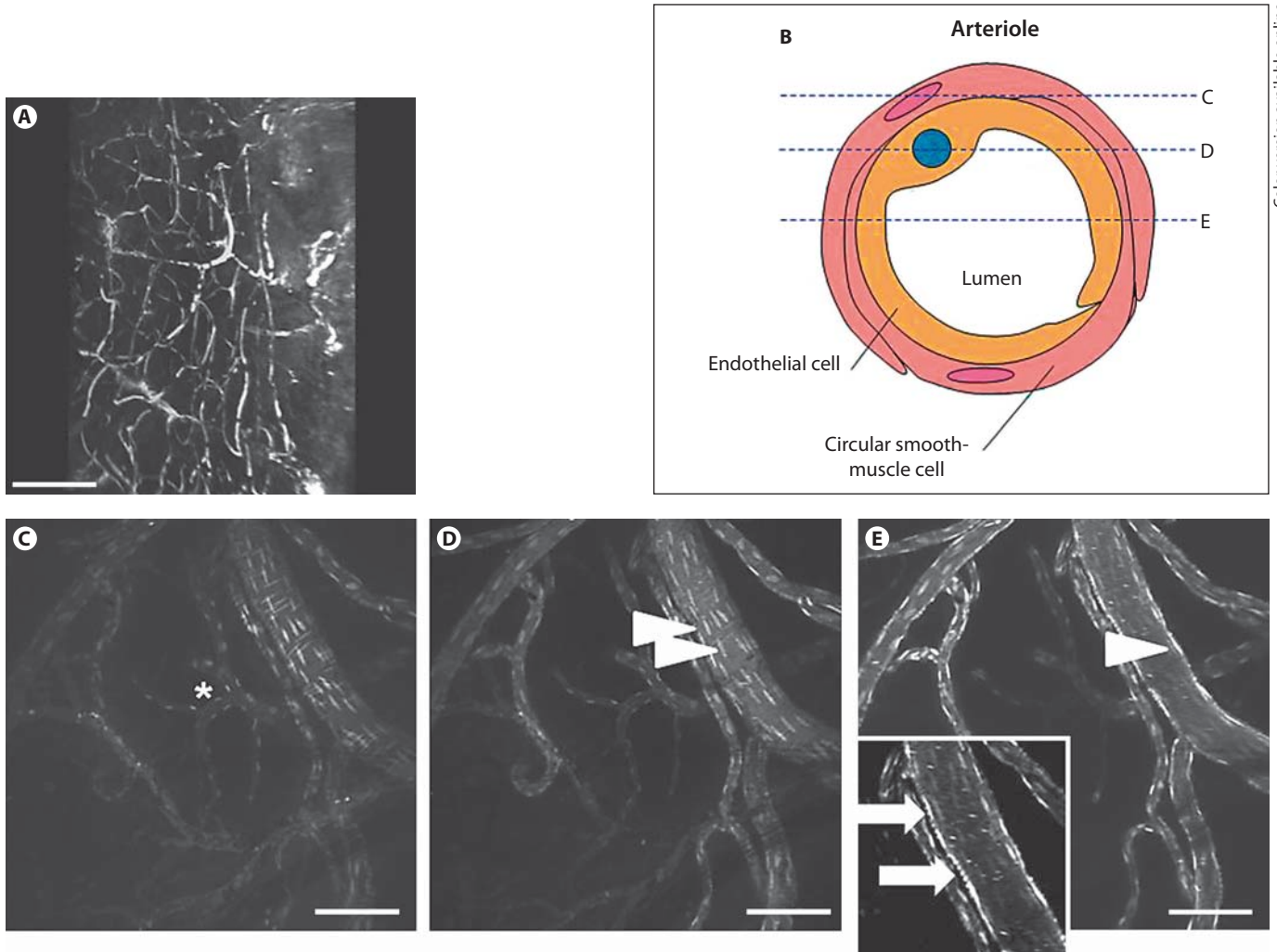
Fig. 1. Brain microvasculature. **A** Visualization of the mouse brain capillary network after injection of FITC-dextran. Three-dimensional reconstruction was performed from a series of consecutive optical sections at 4-μm intervals and captured at an oblique angle. (Animated reconstructions are given as online suppl. fig. 1 and 2, www.karger.com/doi/10.1159/000148242.) **B–E** Brain microvasculature in a gerbil. **B** Scheme of an arteriole. High-resolution optical sections at different depths (**C–E**) are indicated after nuclear labelling with acriflavine, plasma staining with FITC-dextran and injection of labelled RBCs. The arteriole is characterized by transverse bands of smooth-muscle cells resulting in tiny retractions of the vessel wall. Nuclei of the circular smooth-muscle cells (arrows) are clearly differentiated from the nuclei of the endothelial cells (arrowheads) lining the lumen of the arteriole. White dots of the vessel wall (inset in **E**) correspond to transverse optical sections through the circular smooth-muscle cell nuclei oriented circumferentially, endothelial cell nuclei run parallel to the vessel axis. Note the lack of muscle cells in the marked venule (*). Scale bars = 100 μm.

dark clot in repeated serial sections over an observation period of more than 30 min. Thrombotic material of the size of a single cell extended into upstream capillaries.

Visualization of Leucocyte-Endothelium Interaction and Targeted Staining of Single Cells

As the microscopy system used is capable of monitoring microscopic events on a single-cell basis, homing of blood mononuclear cells to vessel walls in the brain of the gerbil was observed over time following sequential triple labelling with acriflavine, FITC-dextran and administration of labelled RBCs (fig. 3A–C). This approach allowed differentiation of nucleated blood cells and erythrocytes and at the same time visualization of blood flow and the vessel wall nuclear structure, which in turn allows identification of arterioles from venules and capil-
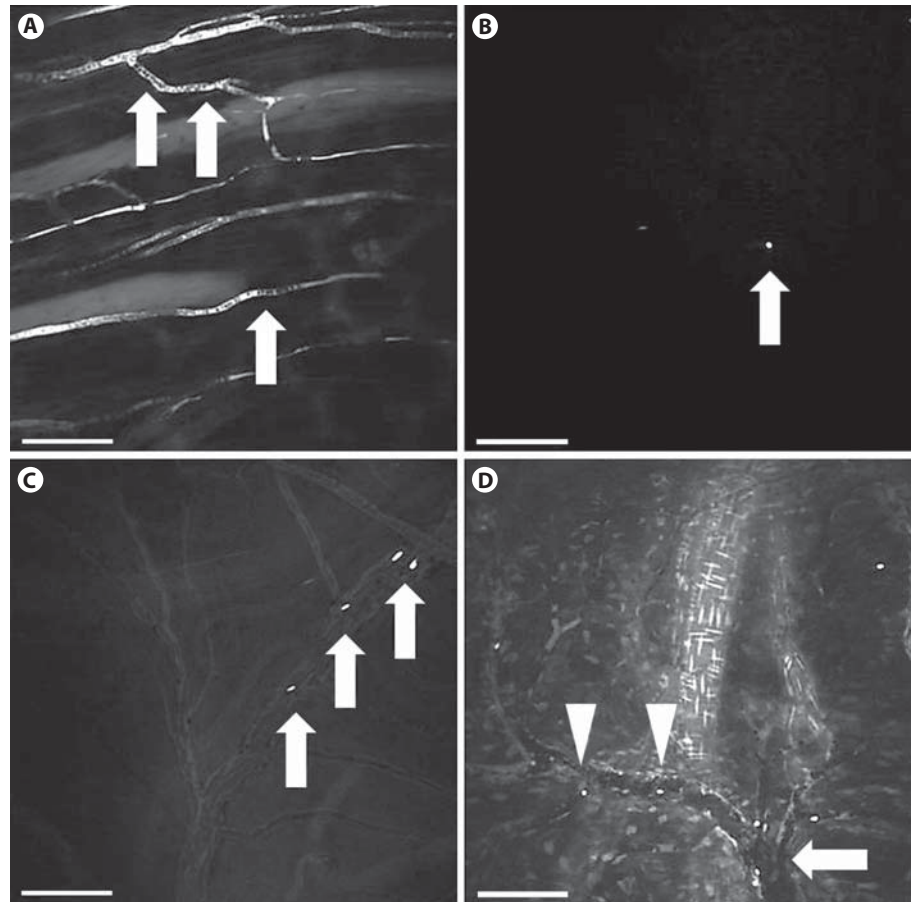
Fig. 2. Single, double and triple staining of microvasculature. **A** After injection of FITC-dextran, single capillaries in the mouse mesentery are selectively highlighted. Unstained blood cells are unlabelled and appear dark within the lumen (arrows), allowing a semi-quantitative assessment of blood flow. **B** An individual FITC-labelled erythrocyte contrasts strongly against the unstained background in a brain vessel of a gerbil (arrow). **C** When blood plasma counterstaining with low concentrations of FITC-dextran is performed at the same site in combination with the administration of FITC-labelled RBCs, unstained blood cells appear in negative (black) contrast, while stained RBCs are still clearly visible (arrows) and contrasted against the background plasma labelling. **D** Thrombosis in a gerbil brain venule after triple staining. Intravenous acriflavine labelling of the nuclei of the vascular endothelial cell nuclei and circular smooth-muscle cell nuclei allow identification of the arterioles and venules. Normal patent vessels are perfused with FITC-dextran-labelled plasma (e.g. arteriole in the centre). A venule containing a microthrombosis (arrow) is characterized by blood stasis (exclusion of labelled plasma flow) and an intraluminal mass of dark unlabelled RBCs containing trapped labelled RBCs (arrowheads). Thrombotic material extends into upstream capillaries. Scale bars = 100 μm.

laries. In sequential images, adhesion of 2 nucleated blood cells to the vessel wall was followed, and these were identified in vivo as mononuclear cells by the high optical resolution of the instrument.

To further corroborate such observations of single cells, PBMCs were visualized in different organs of the mouse after ex vivo staining and re-injection. In vivo observation was easily feasible against a faint background staining with fluorescein, sufficient for reliable tissue characterization (fig. 3D). Where fluorescein alone was administered, such a specific signal within the kidney parenchyma of the mouse was absent (fig. 3E). Uniform staining of individual cells by their molecular properties yielded a fluorescent signal sufficient for intravital cell identification, as shown for FITC-labelled CD3+ cells within the acriflavine-stained liver (fig. 3F).

Imaging of Perivascular Inflammation
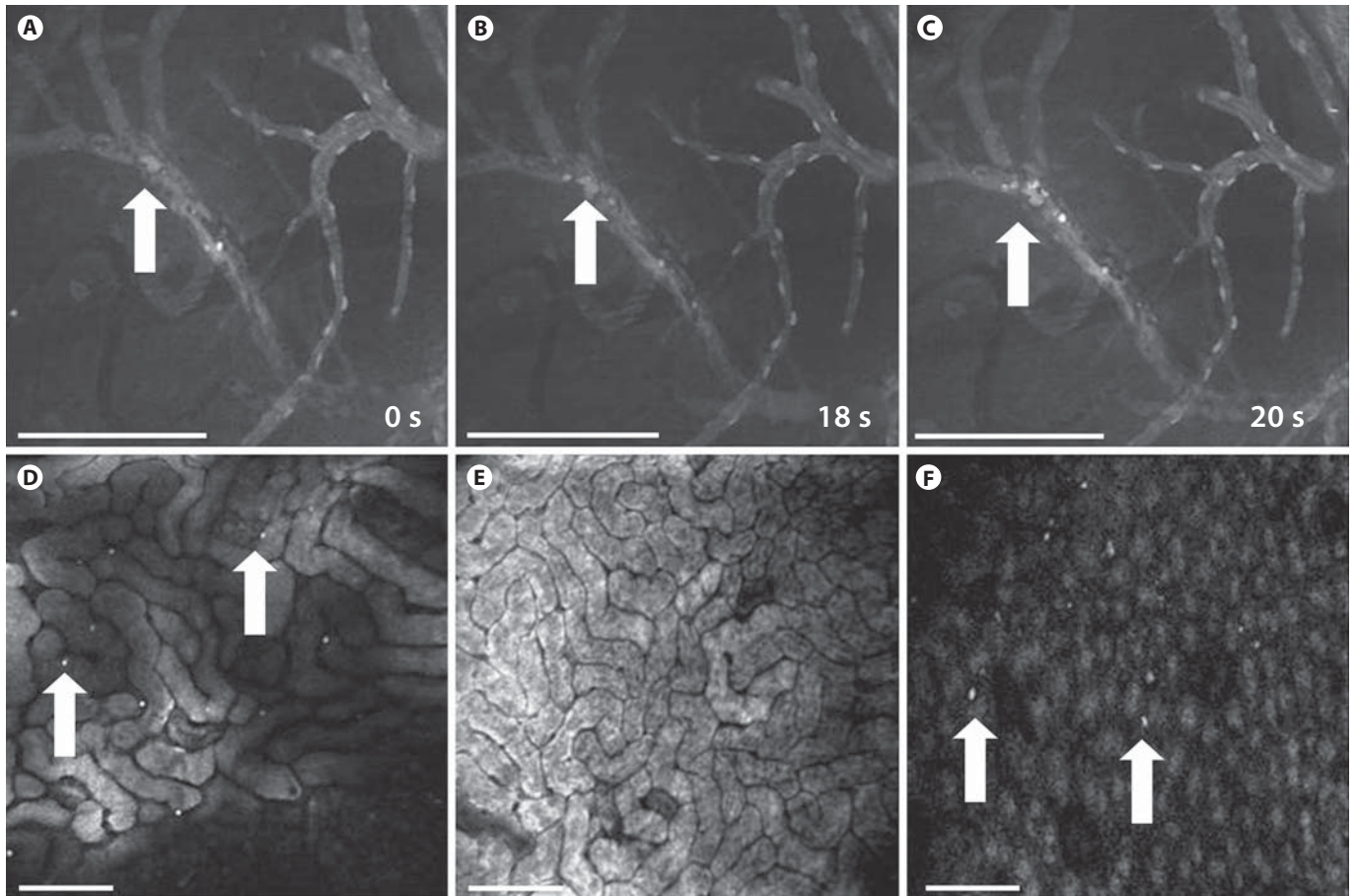To assess the capability of intravital hand-held confocal microscopy for differentiation of normal versus path-

Fig. 3. Blood cell tracking. **A–C** Visualization of leucocyte-endothelium interaction was observed in a brain vessel after sequential injection of acriflavine, FITC-dextran and FITC-labelled erythrocytes. Two acriflavine-labelled mononuclear cells, stained faintly white with prominent intranuclear granules (arrow), are located at the vessel wall. Labelled plasma is shown flowing past both sides, suggesting an only weak interaction with the endothelium. Then, 18 s (**B**) and 20 s (**C**) later, plasma and erythrocyte flows (FITC-labelled erythrocytes, arrows) are limited to one side within the vessel due to the cell-endothelium interaction. **D, E** Acriflavine-labelled PBMCs (arrows) can be visualized selectively in capillaries of the kidney (see also fig. 4A, B) against a faint fluorescein tissue stain (**D**), whereas after intravenous monostaining of the kidney parenchyma with fluorescein, such a specific signal is absent and capillaries appear as black linings around the tubuli. **F** Individual lymphocytes (arrows) are labelled by FITC-labelled anti-CD3 and visualized in the acriflavine-stained liver. Scale bars = 100 μm.

ological vascular structures, a murine model of lupus nephritis was examined. In the healthy murine kidney, plasma labelling with FITC-dextran highlighted the lumen of capillaries surrounding densely packed tubules (fig. 4A). The capillary walls were selectively visualized after labelling the vascular endothelial cells by injection of FITC-labelled *L. esculentum* lectin (fig. 4B), whereas fluorescein equally distributed throughout the parenchyma (fig. 3E). In contrast to the brain, acriflavine diffused out of the vessels in the periphery and labelled nuclei and to a lesser extent the cytoplasm of cells in the renal tubules (fig. 4C). The medullar components of

Henle's loop and the collecting tubules as well as individual glomeruli could be identified (fig. 4D). In the MRL/lpr murine model of lupus nephritis, confocal microscopy allowed visualization of significantly enlarged and thickened Bowman's capsules containing oedematous glomerular vessel loops (fig. 4E). Tubular inflammation was identified by oedematous swelling and peritubular inflammatory infiltration. Ex vivo staining of tissue confirmed the presence of glomerulonephritis, but the oedema was less pronounced as compared to the in vivo situation probably due to tissue retraction upon fixation (fig. 4F).
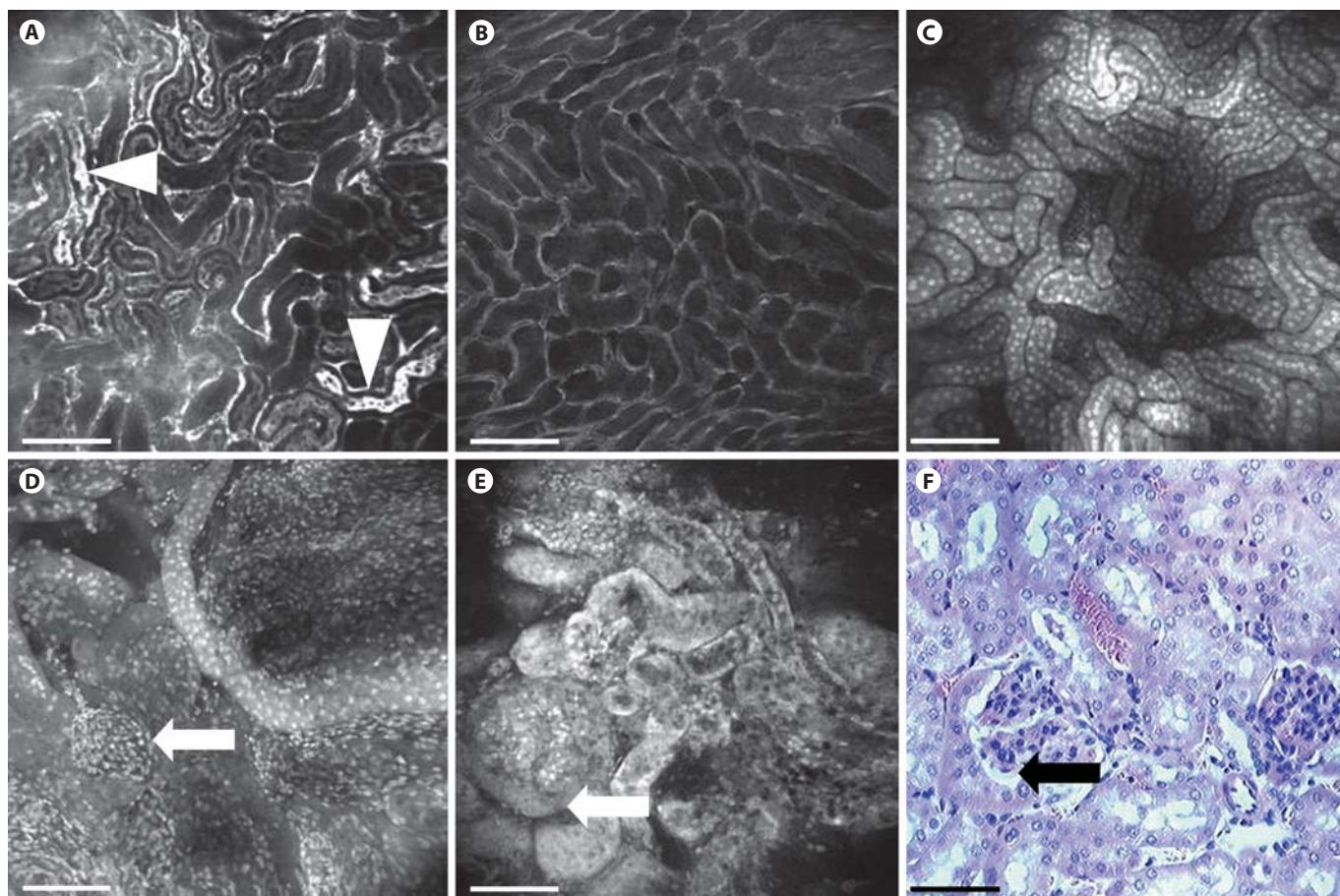
Fig. 4. **A** In the healthy murine kidney, the tubules are densely packed, and the peritubular capillaries are clearly displayed after plasma labelling with FITC-dextran, which is partly excreted into the lumen of the tubule (arrowheads). **B** Similar information is obtained after selectively contrasting the vessel walls with *L. esculentum* lectin. **C** Brightly stained nuclei line densely packed tubules after staining with acriflavine, and in contrast to brain imaging, acriflavine diffused readily out of the microvasculature into the tissue of the periphery. **D** Vessel loops completely fill a glomerulus (arrow). In contrast, glomerulonephritis in a 7-month-old MRL/lpr mouse is characterized by enlarged and oedematous glomerular vessel loops. **E** Bowman's capsule is significantly thickened (arrow), tubule cell nuclei are blurred. **F** Ex vivo HE staining reveals swelling of Bowman's capsule. Oedema of the vessel loops can only be guessed by the retraction of loops from the glomerular border, probably due to a fixation artefact (arrow). Scale bars = 100 μm.

Discussion

A rapid imaging technique of whole tissue such as confocal microscopy allows a plethora of microscopic and cellular analyses in clinical and basic science. However, conventional benchtop confocal microscopes to visualize vasculature, blood flow and cellular interactions in animal disease models are limited by the requirement to bring the animal tissue into precise and stable alignment with the stationary and bulky optics of the microscope. Thus, relatively few studies have successfully applied confocal microscopy to whole animals in vivo. Most studies rather used tissue specimens or sections that may not be adequate to monitor dynamic events, and ex vivo micro-architectural changes have been demonstrated to occur very rapidly after tissue preparation [11].

For intravital vascular imaging in the present study, we evaluated a novel probe that was miniaturized in a way to allow hand-held high-resolution confocal imaging in vivo. With this technique, subsurface imaging at variable penetration depths was achieved, and minute details such as nuclear morphology were clearly resolved in vivo. Differential fluorescent staining protocols permitted simultaneous rendering of distinct features of normal vas-

culature, blood flow and cellular interaction in vivo at high resolution. In vivo resolution of vascular function was suggested by different diffusion patterns of acriflavine: it was clearly confined to labelling of the vessel walls within the brain due to an intact blood-brain barrier, whereas diffusion out of the leakier microvasculature of the kidney resulted in complete parenchymal staining. Pathologies such as a thrombosis of a brain venule and (peri)vascular alterations in a murine model of lupus nephritis were diagnosed. Fixation artefacts that may impede such imaging ex vivo did not play a role in this intravital imaging modality. Although this imaging required an invasive access to the organs investigated, the integrity of the tissue of interest itself was maintained. Thus, continuous imaging of individual cells in their natural environment was feasible at high resolution in sequential sections. In a similar approach, enhanced vessel leakiness in inflamed and malignant tissue has been demonstrated by in vivo visualization of extravasating FITC-labelled dextrans [12], and perfusion abnormalities after thermal ablation of liver tissue have been described in vivo [13]. In the present experiments, such visualization of blood plasma flow was combined with nuclear labelling and targeted staining of specific cell types. Multilabelling was performed using a single-channel instrument with the same excitation and detection wavelengths for all different stains. While this approach does not allow co-localization experiments at different wavelengths, compelling morphological and functional data were provided in vivo by optimizing the concentrations of the individual fluorescent compounds (and re-injection during the examination under direct microscopic monitoring, if necessary). The labelled target structures could be readily distinguished morphologically and by the relative fluorescence intensities of the contrast agents used. Recently, this scanner system has been integrated into a flexible colonoscope, allowing high-resolution microscopy of the human gastro-intestinal tract in vivo [7, 14–16]. Confocal microscopy with a miniaturized probe therefore bears great potential to promote intravital imaging of dynamic processes for vascular research in its natural environment in animal studies and in humans.

In conclusion, confocal microscopy with a novel probe combines for the first time high-resolution subsurface imaging with a time axis for dynamic intravital visualization of vessels, cells, blood flow and associated pathologies. This permits a truly comprehensive vascular imaging, bearing great potential for a deeper understanding of vessel micro-architecture and cellular function and interactions in vivo.

References

1 Stephens DJ, Allan VJ: Light microscopy techniques for live cell imaging. Science 2003;300:82–86.
2 Müller M: Introduction to Confocal Fluorescence Microscopy. Bellingham, Society of Photo-Optical Instrumentation Engineers, 2006.
3 Delaney PM, Harris MR: Fibreoptics in Confocal Microscopy. New York, Plenum Press, 1995, pp 515–523.
4 Wright SJ, Wright DJ: Introduction to confocal microscopy. Methods Cell Biol 2002;70: 1–85.
5 Goetz M, Fottner C, Schirrmacher E, et al: In-vivo confocal real-time mini-microscopy in animal models of human inflammatory and neoplastic diseases. Endoscopy 2007;39: 350–356.
6 Goetz M, Memadathil B, Biesterfeld S, et al: In vivo subsurface morphological and functional cellular and subcellular imaging of the gastrointestinal tract with confocal mini-microscopy. World J Gastroenterol 2007;13: 2160–2165.

7 Kiesslich R, Goetz M, Angus EM, et al: Identification of epithelial gaps in human small and large intestine by confocal endomicroscopy. Gastroenterology 2007;133: 1769–1778.
8 Watanabe-Fukunaga R, Brannan CI, Copeland NG, Jenkins NA, Nagata S: Lymphoproliferation disorder in mice explained by defects in Fas antigen that mediates apoptosis. Nature 1992;356:314–317.
9 Hauck EF, Apostel S, Hoffmann JF, Heimann A, Kempski O: Capillary flow and diameter changes during reperfusion after global cerebral ischemia studied by intravital video microscopy. J Cereb Blood Flow Metab 2004;24:383–391.
10 Holtmann MH, Douni E, Schutz M, et al: Tumor necrosis factor-receptor 2 is up-regulated on lamina propria T cells in Crohn's disease and promotes experimental colitis in vivo. Eur J Immunol 2002;32:3142–3151.
11 Campo-Ruiz V, Lauwers GY, Anderson RR, Delgado-Baeza E, Gonzalez S: In vivo and ex vivo virtual biopsy of the liver with near-infrared, reflectance confocal microscopy. Mod Pathol 2005;18:290–300.

12 Goetz M, Vieth M, Kanzler S, et al: In vivo confocal laser laparoscopy allows real time subsurface microscopy in animal models of liver disease. J Hepatol 2008;48:91–97. DOI: 10.1016/j.jhep.2007.07.029.
13 Nikfarjam M, Muralidharan V, Malcontenti-Wilson C, McLaren W, Christophi C: Impact of blood flow occlusion on liver necrosis following thermal ablation. Aust NZ J Surg 2006;76:84–91.
14 Kiesslich R, Burg J, Vieth M, et al: Confocal laser endoscopy for diagnosing intraepithelial neoplasias and colorectal cancer in vivo. Gastroenterology 2004;127:706–713.
15 Kiesslich R, Goetz M, Vieth M, Galle PR, Neurath MF: Technology insight: confocal laser endoscopy for in vivo diagnosis of colorectal cancer. Nat Clin Pract Oncol 2007; 4:480–490.
16 Polglase AL, McLaren WJ, Skinner SA, et al: A fluorescence confocal endomicroscope for in vivo microscopy of the upper- and the lower-GI tract. Gastrointest Endosc 2005;62: 686–695.